NATIONAL PHYSICAL LABORATORY

MCNP Calculations of Correction Factors for Radionuclide Neutron Source Emission Rate Measurements using the Manganese Bath

by

N J Roberts

Centre for Ionising Radiation Metrology

May 2001

ABSTRACT

The manganese bath method for measuring the neutron emission rate of radionuclide sources requires corrections to be made for emitted neutrons which are not captured by manganese nuclei. The Monte Carlo particle transport code MCNP has been used to calculate the fractions of neutrons that escape from the boundaries of the tank, that are captured by the steel cavity in which the source is housed, and that are captured by fast neutron reactions in oxygen and sulphur in the solution. A comparison has been made with the calculations from the in-house transport codes, and the measurements with the long counter, which highlighted a number of disagreements. These have been investigated and satisfactorily explained. Validation work has also been performed to demonstrate the reliability of the model. In future, the MCNP model will be used, in place of the in-house codes and the long counter, to calculate the correction factors.

ISSN 1369-6793

National Physical Laboratory
Teddington, Middlesex, UK, TW11 0LW

Approved on behalf of Managing Director NPL, by Dr Martyn Sené
Head, Centre for Ionising Radiation Metrology

CONTENTS

1 INTRODUCTION

Radionuclide neutron source emission rates have been measured at the National Physical Laboratory for the last forty years, and a Measurement Service for determining emission rates is currently offered by the Centre for Ionising Radiation Metrology. The service is available to customers on a fee-paying basis and is used by industry, research laboratories, universities and hospitals. Sources measured at NPL are in use throughout the UK and in many countries overseas. These radionuclide sources, together with knowledge of their neutron energy spectrum, form the basis of the calibration of secondary standard instruments, such as the Precision Long Counter, and are extensively used for the calibration of neutron detectors, area survey instruments, and personal dosemeters.

Absolute measurements of the neutron emission rate from radionuclide neutron sources are made at NPL by the manganese sulphate bath technique. The quantity measured is the total neutron emission into 4π sr. Source neutrons are captured by the manganese in the solution to produce ^{56}Mn activity which is subsequently detected to determine the source emission rate. However, not all emitted neutrons are captured by the manganese and the magnitude of these losses must be determined by either calculation or measurement.

Since the development of the Manganese Bath at NPL, losses to fast neutron reactions in oxygen and sulphur and capture by the source and source cavity had been calculated using a combination of a Monte Carlo and a diffusion modelling code. Both codes were written in-house and for many years they did an excellent job, particularly in view of the limited computing power available. Recent advances in computer speed and the availability of superior external Monte Carlo codes have provided the opportunity to check and improve the accuracy of the calculations and hence reduce the uncertainty in the primary standard of neutron emission rate.

Modelling of the bath was carried out about 6 years previously, using the Monte Carlo code MCNP (version 3A), but the transition to using MCNP to calculate the losses on a permanent basis was never made. Instead the modelling work served only as a check of the existing codes. The work described in this report carries on from the previous work in that the model is essentially the same having only undergone minor alterations, but now version 4B of MCNP has been used with a newer set of cross section tables (ENDF/B-VI[He94]).

2 THE MANGANESE BATH

The manganese bath technique, as implemented at NPL, involves placing the neutron source at the centre of a spherical tank of concentrated aqueous solution of pure manganese sulphate ($MnSO_4$) with a hydrogen to manganese atom ratio $N_H/N_{Mn} \approx 30$. The tank (98cm in diameter) is sufficiently large to ensure almost complete absorption of the emitted neutrons. Approximately 50% of the source neutrons are captured by manganese nuclei forming ^{56}Mn, which decays to ^{56}Fe.

$$^{55}\mathrm{Mn} + \mathrm{n} \rightarrow {}^{56}\mathrm{Mn} \rightarrow {}^{56}\mathrm{Fe} + \gamma + \beta^-$$

The decay of ^{56}Mn has a half-life of (2.579 ± 0.003) hours[Sm95]. The solution is continuously stirred and pumped through the detector systems which consist of a pair of NaI scintillators mounted in re-entrant wells in the ends of cylindrical vessels through which the circulating solution passes.

The growth of activity in the tank, and hence the count rate observed in the NaI detector channels, does not exactly follow a (1-exp[-λt]) curve due to the circulation of the solution through the counting system. While circulating, the solution is not being irradiated by neutrons. The time taken to travel from the bath to the detectors and back again is about 3 minutes for the higher efficiency channels, and 1 minute for the lower efficiency channels. In this time the activity of the circulating solution decays by approximately 1.4 and 0.5 % for the higher and lower efficiency channels respectively. Therefore the solution that is reintroduced to the tank has a lower activity than the solution already in the tank. As a result, the overall increase in activity is slower than may be expected. This process is allowed for by the manganese bath data analysis program and is explained in more detail in the paper by Axton[Ax65].

The counts from the NaI detector channels are recorded for fixed cycle times, usually of 1000 seconds each. Every count cycle of the growth in activity is used to calculate values for the saturation count rate. The same process is carried out for the decay in activity once the source has been removed from the bath. A mean value for the count rate at saturation (A) is obtained and used in the following formula to calculate the neutron emission rate (Q):

$$Q = \frac{A}{\varepsilon f (1 - O - S - L)} \qquad (1)$$

where: ε is the detection efficiency of the system in recorded counts per disintegration occurring anywhere in the system.
f is the fraction of thermal neutrons captured by manganese in the solution as opposed to those captured by other nuclei (H, S, impurities).
(1-O-S-L) is a correction for other neutron losses discussed in detail in section 3.

3 CORRECTION FACTORS

The correction for thermal neutron capture by nuclei other than manganese (f) is independent of the neutron energy spectrum of the source, the solution concentration, and the geometry of the source, cavity, and bath. This greatly simplifies its determination and it can therefore be calculated using the equation of Westcott[We58]. The (1-O-S-L) correction includes three components, all of which are dependent on the source energy spectrum, solution concentration, and the apparatus geometry:

O = the fraction of source neutrons undergoing (n,α) reactions in oxygen, and (n,α) and (n,p) reactions in sulphur, in the solution.

S = the fraction of source neutrons captured in the neutron source (having previously left the source), and the cavity assembly.

L = the fraction of source neutrons which escape from the boundaries of the bath.

The dependence of these corrections on so many factors means that modelling is required, although in the case of L, a flat-response detector has been used to measure the leakage. An in-house Monte Carlo code is available which tracks neutrons from the source (starting with the appropriate energy spectrum) to a point in the bath where their energy can be taken as thermal. Any (n,α) and (n,p) reactions in oxygen and sulphur are logged by the code enabling the capture fraction (O) to be calculated.

The positions in the bath where the source neutrons become thermal is then fed into another code which applies diffusion laws to the transport of neutrons. The second code calculates how many will be scattered from the solution back into the cavity and uses the capture cross sections for steel and for the source material to predict what fraction of neutrons will be lost to the cavity and the source (S).

For simplicity, the codes treat the bath, source, and cavity as being spherically symmetric. The thermal neutron fluence in and around the cavity is determined and then multiplied by cross sections for the cavity, source capsule and cup, and source material. An important consequence of this is that the stainless steel rod which positions the cavity at the exact centre of the bath could not easily be included in the calculations. It is likely that when the codes were written a cord based system was used for positioning the cavity, and so it was not necessary to consider capture by components outside of the cavity itself.

Another simplification was to take mean energy values for the capture cross sections of steel and the source material. A proper treatment would consider both the incident neutrons and the cross sections as functions of energy.

A calibration factor is used to convert counts in the flat-response detector (a De Pangher Long Counter) into the number of neutrons lost over the entire 4π sr of the tank. Values for the factor have come from a number of experiments using tanks of different radii[Ax85a] and solutions of different concentrations[Ax85b], as well as from calculations using the thermal diffusion code mentioned earlier. The final value is a mean of all the different methods.

4 MCNP MODELLING

4.1 The Code

MCNP[Br97] is the most widely used general purpose Monte Carlo neutron-photon-electron transport code. The Monte Carlo method does not solve the transport equation at all. Instead it obtains answers by simulating the actual behaviour of particles, using the results to infer the mean behaviour of all particles by the Central Limit Theorem. Monte Carlo is particularly suited to solving complex three-dimensional problems, which would prove difficult or impossible to solve analytically.

There are numerous advantages in using MCNP over the in-house codes, including:

- MCNP has had over 450 person-years of development and has a user base of around 3000 worldwide making it highly unlikely that bugs will go unnoticed.

- MCNP uses the latest continuous energy cross section libraries containing far more information than those used by the in-house codes.
- MCNP allows the geometry to be modelled in detail, avoiding simplifications and approximations.
- MCNP allows other problems with the manganese bath to be studied, such as how sensitive the solution activity is to the exact positioning of the source at the centre of the bath.
- Variance reduction techniques can be used with MCNP to reduce the statistical uncertainty on the correction factors.
- MCNP allows the different neutron interactions to be modelled in far more detail.

However it should also be borne in mind that the results from MCNP are only as reliable as the data given to it, such as geometry, material compositions, and cross section tables. Attention should also be paid to the statistical analysis given in the output file to check the validity of solutions and to avoid false convergences.

4.2 The Model

The model used was originally developed by Olivia Naismith[Na94]. There are three versions corresponding to the different source types (as currently manufactured by AEA Technology) which represent the most common calibrations performed in the bath:

- Californium-252 (spontaneous fission) in an X1 capsule
- Americium-Beryllium (α,n) in an X3 capsule [1 Ci = 37 GBq]
- Americium-Beryllium (α,n) in an X14 capsule [10 Ci = 370 GBq].

All three were modelled inside the small (8.8 cm diameter) cavity sphere, at the centre of the large (98 cm diameter) tank.

The activities, and hence the masses of americium and beryllium, present in the ^{241}Am-Be sources are required only for the calculation of neutron capture by the source material. The emission rate of the sources is irrelevant for the calculation of correction factors. Californium sources contain such a small mass of source material that neutron capture is insignificant.

The grade of stainless steel used throughout the model is 316L. Engineering drawings of the small cavity sphere, source capsules, and source cups specify this grade. The chemical composition of 316L was obtained from the Handbook of Chemistry and Physics[We73], taking mid-point values where a range of percentages by weight were specified for an element.

A hydrogen to manganese atomic ratio (N_H/N_{Mn}) of 33.200 has been used for all runs except those performed as part of the validation where the solution concentration of the bath during the experiment has been used. An atomic ratio of 33.200 is typical of the actual concentration of the solution and corresponds to a solution density of 1.4046 g cm^{-3} (from a fit made to experimental data). Densities at other concentrations were also obtained from the fit. The atomic fractions of the H, Mn, S, and O were calculated from the value of N_H/N_{Mn}.

Plots of the model are shown in Figures 1 and 2. It can be seen that the neck and lid of the tank have not been included in the model. This was a simplification made in the original model to save on run time. Instead, the part of the sphere where the neck is located has been assigned a higher density to account for the greater thickness of the lid. The geometry of the source capsules was also simplified in the original model to be an exact cylinder ignoring features at the ends, such as a threaded hole in the case of the X3 and X14 capsules. Neither of these simplifications altered the results [Na94] and so they have remained in the model for this work.

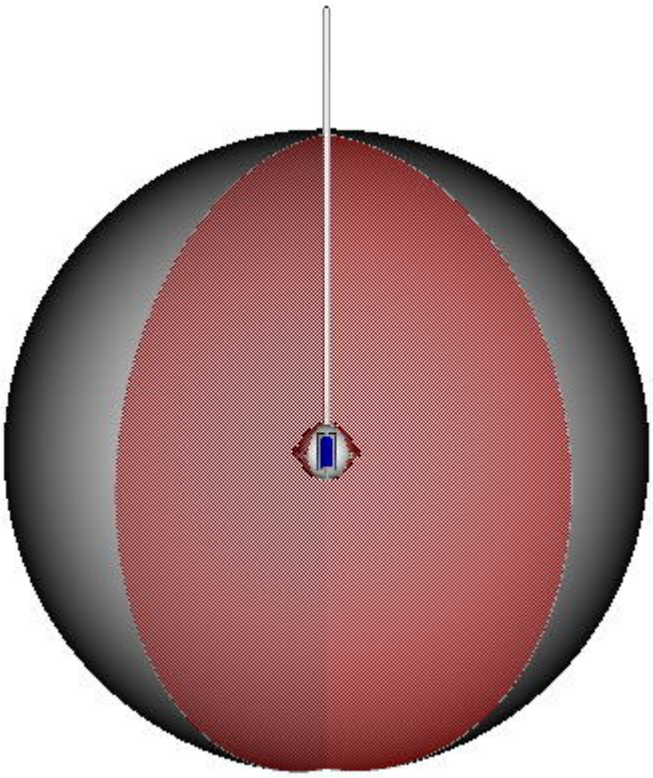

Figure 1: 3D plot of the MCNP geometry of the manganese bath with section removed

Key:	Red	=	$MnSO_4$ solution
	Blue	=	Source material
	Grey	=	Stainless steel
	Green	=	Rubber
	White	=	Vacuum (void)

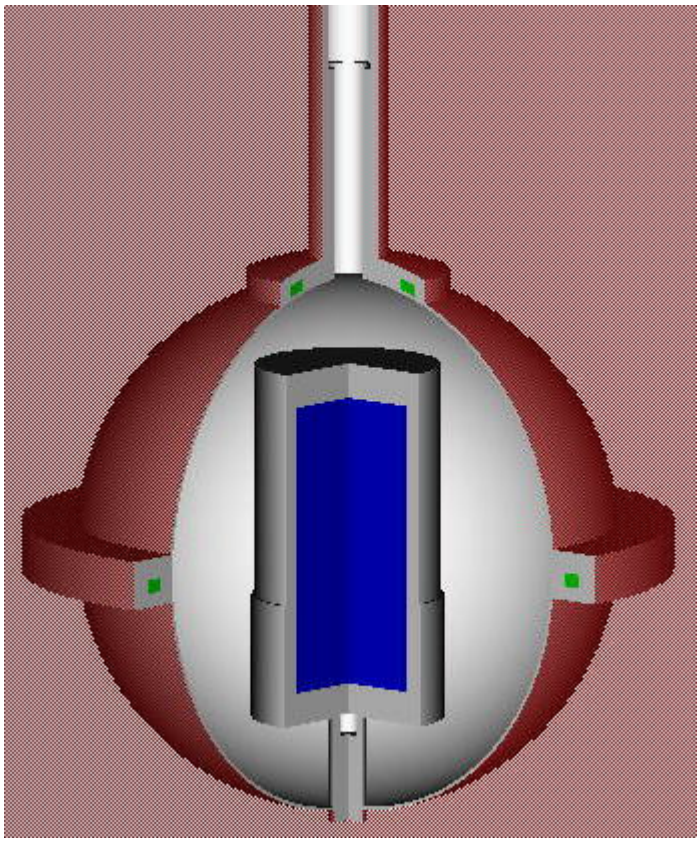

Figure 2: Enlargement of the source cavity containing an X14 capsule

Although the geometries of the source capsules have been modelled in detail, for the purposes of MCNP, a spherical surface distribution lying just outside the source capsule has been used as a source definition. Defining the source this way ensures that all tallies are *per neutron emitted from the source* (i.e. normalised to those that leave the exterior surface of the capsule). Some neutrons leaving the source material will get captured as they pass through the capsule and these are not included in the source emission rate and therefore should not be considered here. The energy spectra used for the sources are those from ISO 8529[IS89].

The source has been modelled as having isotropic emission, when in reality the emission is anisotropic. To confirm that this simplification made no difference to the calculations, the anisotropic emission of all three sources were added to the respective models. The results agreed with those from an isotropic source to within 0.1%.

In the model, the manganese bath is located in an infinite vacuum. This is another simplification as it does not allow for neutrons which may leave the bath and re-enter. To check that this effect was negligible, the walls, floor, and ceiling were added to the model, as well as the long counter which rests on the side of the tank. There was no difference in the results obtained.

Tallies were run for approximately 1,500,000 histories, with each history corresponding to one particle emitted by the source. On a 350 MHz PC these took about 5 hours to run.

New cross section evaluations are available with MCNP-4B that were not available with version 3A run previously. The different evaluations used are shown in table 1. The in-house codes use epithermal cross sections from the Saclay Data Centre[Sa73], and thermal capture cross sections from E J Axton[Ax86].

Table 1: Sources of cross section data

Element	MCNP-4B		MCNP-3A	
	ZAID	Library	ZAID	Library
H	1001.60C	ENDF-VI	1001.04C	ENDF/B-IV
Be	4009.60C	ENDF-VI	4009.03C	LASL
C	6012.50C	RMCCS B-V	6012.35C	ENDL-85
O	8016.60C	ENDF/B-VI	8016.04C	ENDF/B-IV
Si	14000.60C	ENDF/B-VI	14000.35C	ENDL-85
P	15031.60C	ENDF/B-VI	15031.35C	ENDL-85
S	16032.60C	ENDF/B-VI	16032.35C	ENDL-85
Cr	24000.50C	RMCCS B-V	24000.35C	ENDL-85
Mn	25055.60C	ENDF/B-VI	25055.35C	ENDL-85
Fe	26000.55C	RMCCS T-2	26000.35C	ENDL-85
Ni	28000.50C	RMCCS B-V	28000.11C	ENDF/B-IV
Mo	42000.60C	ENDF-VI	42000.35C	ENDL-85
Am	95241.60C	LANL	95241.35C	ENDL-85

The following tallies were defined in the input file:

- Neutron leakage from bath [tally number 1]
  Using a type 1 (surface current) tally on a sphere located outside the boundary of the tank. Type 1 tallies log the number of particles crossing the surface in any direction.

- Thermal energy spectrum inside cavity [11]
  Using a type 1 tally on the interior surface of the cavity sphere, broken down into energy bins.

- Thermal energy spectrum outside cavity [21]
  As 11 but on the exterior surface of the cavity sphere.

- Neutron capture in cavity [4]
  Using type 4 (track length estimate of cell flux) tally on all the stainless steel cells that comprise the cavity (e.g. cavity sphere, transport rod, source capsule, source cup). An FM tally multiplier card is used to convert track length to number of neutrons undergoing capture in the material.

- Neutron capture in rubber seal [14]
  Using type 4 tally on the O-ring between the two hemispheres of the cavity, with an FM card.

- Neutron capture in $MnSO_4$ solution [24]
  Using type 4 tally with an FM card.

- (n,γ) capture in manganese [34]
  Using type 4 tally, with an FM card specifying the number density of manganese in the solution and that only interactions with manganese nuclei (not all nuclei in the solution) should be tallied.

- Neutron capture in sulphur: Total, (n,γ), (n,p), (n,α) [44]
  Using type 4 tally, with an FM card specifying sulphur and broken down into the different reaction types.

- Neutron capture in oxygen: Total, (n,γ), (n,α) [54]
  As 44 but specifying oxygen.

- (n,γ) capture in hydrogen [64]
  As 34 but specifying hydrogen.

The number densities used in the FM cards were obtained from the table of cell details in the MCNP output file. For the elements which are not directly used in a cell (i.e. Mn, S, O, H), the number densities were calculated from the $MnSO_4$ solution number density using the atomic fractions. All number densities are given in units of atoms per barn cm (i.e. atoms per 10^{-24} cm^3).

5 RESULTS FROM MODELLING

5.1 Comparison of correction factors

The MCNP model was run to provide a direct comparison with the in-house codes and long counter for the standard cases. Table 2 shows the results obtained for the three capture and loss methods (O, S, and L) expressed as percentages of neutrons emitted by the source. Significant disagreement can be seen for O and S, both of which have been underestimated by up to 0.8%. Table 3 shows the effect these differences have on the combined correction factor. As the factor appears as a multiplier in equation 1, the percentage increases with MCNP also apply directly to the calculated source emission rates.

Table 2: Comparison of capture & loss percentages for the standard cases

Source/capsule	O & S (n,p) (n,α) [O]		Source & cavity [S]		Leakage [L]	
	MCNP-4B	In-house	MCNP-4B	In-house	MCNP-4B	Long counter
^{252}Cf X1	0.82%	0.66%	1.89%	1.30%	0.36%	0.38%
^{241}Am-Be X3	3.34%	2.79%	1.56%	0.99%	1.41%	1.56%
^{241}Am-Be X14	3.33%	2.79%	2.12%	1.32%	1.36%	1.56%

Table 3: Comparison of combined correction factors for standard cases

Source/capsule	$\frac{1}{(1-O-S-L)}$		Percentage increase with MCNP-4B
	MCNP-4B	In-house, long counter	
^{252}Cf X1	1.0317	1.0240	0.75
^{241}Am-Be X3	1.0674	1.0564	1.04
^{241}Am-Be X14	1.0731	1.0601	1.23

5.2 Oxygen and sulphur fast neutron capture [O]

A breakdown of the oxygen and sulphur fast neutron capture is given in table 4. It shows that the O(n, α) reaction is mainly responsible for the disagreement.

Table 4: Breakdown of oxygen and sulphur fast neutron capture

Reaction	^{252}Cf X1		^{241}Am-Be X3		^{241}Am-Be X14	
	MCNP-4B	In-house	MCNP-4B	In-house	MCNP-4B	In-house
O(n, α)	0.56%	0.38%	2.65%	1.81%	2.64%	1.81%
S(n, α),(n,p)	0.25%	0.28%	0.69%	0.98%	0.69%	0.98%

The previous work of Naismith had found good agreement between MCNP and the in-house codes for fast neutron capture. This can be explained by the newer cross section libraries used in this work (see table 1).

The present models were run again but this time specifying an older cross section library for oxygen (RMCCS B-V as ENDF/B-IV is unavailable with MCNP-4B). The O(n, α) capture fractions were 0.41% and 1.85% for ^{252}Cf X1 and ^{241}Am-Be X3 respectively. These are in excellent agreement with the values from the in-house codes which also use older cross section tables.

Further to this, the ENDF/B-VI cross sections for O(n, α), S(n, α), and S(n,p) were rebinned into the 243 bin structure used by the in-house code BATHMCARLO. The code then gave oxygen and sulphur fast capture fractions of 2.95% and 0.76% respectively for the ^{241}Am-Be X3 case which agree reasonably well with the values obtained using the same cross sections in MCNP.

Plotting the Saclay 1973 cross sections with the ENDF/B-VI data shows that the newer values are considerably greater particularly at higher energies (see figure 3). The ENDF/B-VI evaluation of neutron cross sections for ^{16}O was carried out by Hale et al[Ha91]. New measurements of the total cross section were included which implied a different normalization for the (n, α) cross sections than that obtained in the ENDF/B-IV analysis. It is this renormalization that has increased the calculated O(n, α) capture fraction, as opposed to any fault with the in-house Monte Carlo code.

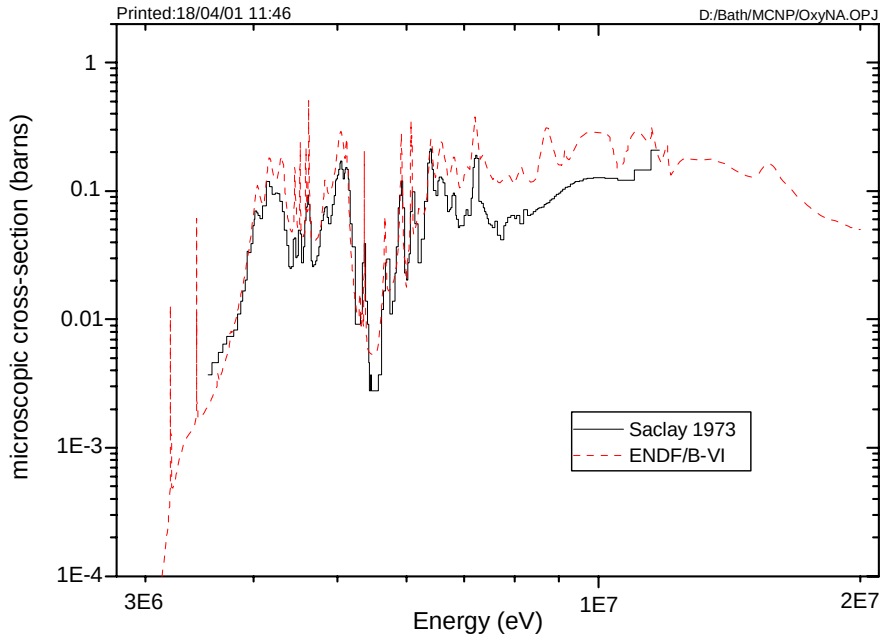

Figure 3: Plot of ENDF/B-VI O(n,α) cross sections, used by MCNP-4B, and Saclay data, used by the code BATHMCARLO

5.3 Source and cavity capture [S]

Breaking down the source and cavity capture into its component parts (see table 5) reveals that there are two reasons for the disagreement in this correction.

- The transport rod used to move and position the source cavity at the exact centre of the bath was not considered by the in-house code BATHDIFF.
- Capture by all stainless steel components is underestimated by BATHDIFF.

Table 5: Breakdown of cavity capture

	^{252}Cf X1		^{241}Am-Be X3		^{241}Am-Be X14	
	MCNP-4B	In-house	MCNP-4B	In-house	MCNP-4B	In-house
Cavity sphere	1.50%	1.27%	1.03%	0.78%	0.98%	0.56%
Transport rod	0.33%	(not included)	0.25%	(not included)	0.24%	(not included)
Capsule & cup	0.06%	0.04%	0.24%	0.15%	0.46%	0.32%
Source material	-	-	0.05%	0.05%	0.44%	0.44%

As previously stated in section 3, the transport rod was omitted from the in-house codes to simplify the problem as it was wrongly believed that it captured a negligible number of neutrons.

The underestimation of capture by the steel components is mainly due to the underestimation of the thermal fluence inside the cavity by the code BATHDIFF. Measurements with gold foils suggest it could be as much as 25% greater than that calculated by the in-house codes. BATHDIFF makes a correction for flux depression due to the presence of the steel components and there is some doubt as to the accuracy of this. Another possible source of error is the use of a mean capture cross section for steel. In the thermal region, the steel capture cross section has a 1/E shape so the use of a mean value is an oversimplification.

5.4 Leakage from the bath [L]

The fractions of neutrons escaping through the walls of the tank calculated by MCNP are lower than the values obtained by measurements with the long counter for all 3 cases. Being lower, the MCNP correction for leakage will partially cancel out the disagreements in the O and S corrections which were higher when calculated using MCNP.

The reason for the lower value of L is not clear, however the methods used to calibrate the long counter allow significant uncertainties to be introduced in a few places. Conventionally, long counters can be calibrated using a source of known emission rate at a known distance from its effective centre, but neutrons leaking from the manganese bath scatter from the entire volume of the tank so it cannot be treated as a point source.

Assumptions and approximations have to be made about the position of the effective centre, and how the decrease in neutron fluence varies with distance in a moderator in order to use an infinite bath extrapolation technique based on two sizes of bath[Ax85a]. In combination, these make an error of the order of 10 - 15% in the calculated calibration factor quite possible.

One advantage of routinely using the long counter, as opposed to making a calculation of the leakage, is that the calibration of the long counter is independent of the source energy spectrum. If the source material is contaminated (e.g. Be in an ^{241}Am-B source, or ^{250}Cf in a ^{252}Cf source) the energy spectrum will be slightly different and this can alter the fraction of neutrons which escape. The long counter will detect this difference but a calculation based on a standard source energy spectrum will not.

5.5 Use of MCNP version 4C

During this work, a new version of MCNP was released (version 4C[Br00]). The old version (4B) continued to be used, but the models for all 3 source and capsule types were run using the new version for comparison. Agreement between the calculations was better than 0.01%. Version 4C should therefore be used for all future calculations.

6 VALIDATION OF THE MODEL

6.1 Measurements with stainless steel sleeve

To test the model experimentally, manganese bath calibrations of a 10 Ci ^{241}Am-Be source in an X14 capsule (serial number 7245NE) were carried out with and without a stainless steel sleeve placed over the source transfer rod. The sleeve increased the mass of stainless steel in the region of the rod by a factor of 6.5. Both cases were modelled using MCNP-4B, ensuring that the concentration of the $MnSO_4$ solution and the masses of the rod and rod sleeve agreed with the experimental case.

The presence of the sleeve reduces the fraction of source neutrons captured by the ^{55}Mn in the bath and hence the count rate at saturation is reduced by the same relative amount. The cycle data for the measurements were analysed in the same manner as a normal source calibration to yield a mean saturated count rate corrected to a given reference time. The $^{55}Mn(n,\gamma)^{56}Mn$ reaction was tallied directly by MCNP and therefore the modelled decrease could be compared with the actual decrease.

Uncertainties in the ratios for both experiment and model are dominated by a statistical component. Most other uncertainties (e.g. dead-time, efficiency) are common to the measurements made with and without the sleeve and so will cancel out. Some allowances have been made for the geometry of the model and for the cross-section tables used by MCNP. The experimental uncertainty includes a component for timing uncertainties as the sleeve had to be attached after the source was placed in the bath and removed before the source was removed.

The results of the comparison are shown in table 6. There is excellent agreement between the model and the experiment. This validates the results of the model showing that the source transfer rod captures a significant fraction of neutrons and should not be ignored when calculating correction factors. The model's calculations of fast neutron capture and bath leakage are not directly validated by the agreement but this result increases confidence in all aspects of the model.

Table 6: Results of steel sleeve validation

	Experiment	Model
Ratio of Mn capture (with sleeve:without sleeve)	0.9942	0.9945
Uncertainty in ratio (absolute)	0.0007	0.0010
%age decrease in Mn capture due to sleeve	0.58	0.55
Uncertainty in decrease (absolute)	0.07	0.10

6.2 Irradiation of gold foils inside the cavity

Another experiment that allows a modelled quantity to be compared with a measured quantity is the irradiation of gold foils located inside the cavity during a source measurement. Pairs of gold foils (mass 96.5 mg, area 1 cm^2, thickness 0.05 mm) were fixed to a thin perforated steel disc inside the cavity (see figure 4) with a 10 Ci ^{241}Am-Be source in an X14 capsule (serial number 7245NE), and then with a 75 μg ^{252}Cf source in an X35 capsule (serial number 4774NC). Each measurement was repeated with similar foils in the same positions but this time inside cadmium covers to exclude thermal neutrons.

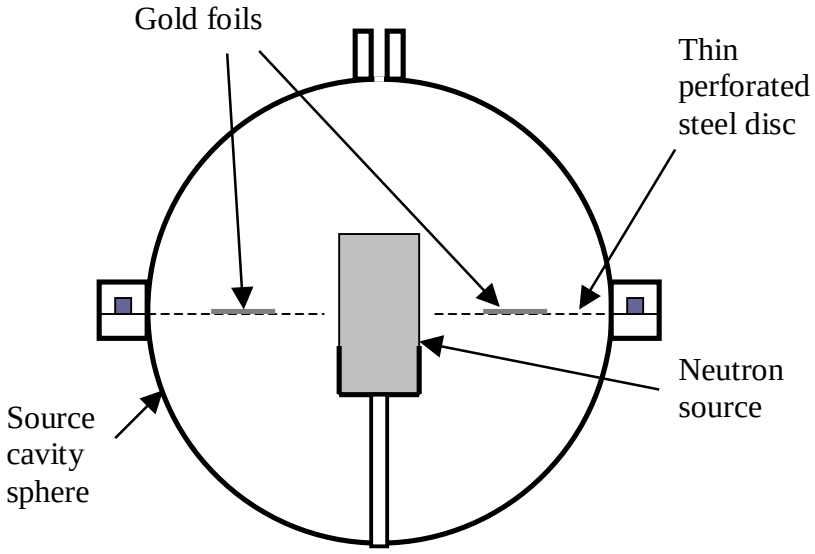

Figure 4: Positions of gold foils inside source cavity (not to scale)

The activities of the irradiated foils were determined by measuring the emitted β particles in anti-coincidence shielded low background counters (see the paper by Axton[Ax63] for more details on the β counting technique). The efficiencies of the foils to both thermal and epithermal neutrons are known from irradiations in a reactor. Dividing the activities at saturation by the emission rate of the source gives the capture per source neutron.

By including the foils in the geometry of the bath model, tallies could be made of the neutron capture in the foils using MCNP. For the ^{252}Cf source, the capsule was modelled as an X1. The small decrease in capsule size from an X35 should not significantly alter the calculated capture in the foil. For both sources the two foils

were modelled as a continuous ring of gold in the same plane to increase the number of neutrons captured in the gold and so improve the statistics of the problem. For simplicity, the steel support disc was modelled as being very thin rather than perforated. The 'weight window' feature of MCNP-4B was used to further improve the convergence of the tally.

Table 7: Comparison of gold foil results

Source	Capture per source neutron per mg ($x10^{-7}$)		Percentage decrease with MCNP-4B
	Experiment	MCNP-4B	
^{241}Am-Be	4.10	3.87	5.6
^{252}Cf	6.73	6.37	5.3

The results given in table 7 show that there was reasonable agreement between experiment and model. Although the statistical components of the uncertainties in the results are small (<1%), there are a number of other factors which limit the accuracy of the capture fractions. For the analysis of the foils the β counting efficiency (ε_β), and the source emission rate in particular combine to give an overall uncertainty of ~2%. The model is limited by the cross section data, and the approximations made to the geometry (e.g. source capsule, continuous foil ring, steel support disc, uncertain positioning of the foils). A conservative estimate of the total uncertainty in the MCNP results would be ~4%.

A difference of ~5% in the model is therefore of little significance. If the model can calculate the fluence in the cavity to within 6%, and hence determine the fraction of neutrons captured by the cavity to the same level of accuracy, then the propagated uncertainty in the source emission rate due to this correction will be very low (<0.15%).

7 UNCERTAINTIES

The overall uncertainty in any MCNP tally is made up of four main components:

- Statistical

  A measure of how well the tally has converged to its final answer. This uncertainty is calculated by MCNP and is given in the output file. It can be reduced by the use of variance reduction techniques (e.g. weight windows) or simply by tracking more particles. The values quoted here are from runs of approximately 1,500,000 histories and do not make use of any variance reduction techniques.

- Cross section

  The probabilities of particle interaction are fundamental to all calculations of transport through material. The accuracy of cross section tables is therefore of great importance. Small changes in the cross sections can significantly alter the tally results. It is only possible to estimate this uncertainty based on the shift in the results when a different set of cross section tables are used. This produced a shift of up to 24% in the case of the O correction for ^{241}Am-Be sources. A lower value of 20% has been assigned for this case using the argument that the newer evaluation should be more reliable than the older

evaluation. For the ^{252}Cf X1 source, an 18% change has been lowered to a 15% uncertainty by applying the same argument.

- Geometry

  In addition to the physical dimensions of the MCNP cells, the densities and compositions of the constituent materials are all important parameters in the calculations. To determine the sensitivity to changes in the geometry, the PERT card was used to perturb material compositions and densities. This gave the tally results both with and without the perturbations present.

  The first perturbation changed the composition of stainless steel in the model. Where previously a mid-point value had been taken if a range of percentages by weight for an element in the steel was specified, in the perturbation the lowest possible percentage was taken. Previously, where a maximum value was listed for the percentage by weight of an element, the maximum was used in the model. In the perturbation these were decreased slightly (~1%). To counteract the decreases in the fractions of the other elements there was a corresponding increase in the fraction of iron. The density was also changed from 7.93 g cm^{-3} to 7.95 g cm^{-3}.

  The second and third perturbations changed the density of the $MnSO_4$ solution from 1.4046 g cm^{-3} to 1.4116 g cm^{-3}, and 1.3976 g cm^{-3} respectively. These represent an uncertainty of ±0.5% in the density which comes from the uncertainty in the fit as well as in the measurement of the solution concentration.

- Source energy spectrum

  The energy of the starting neutrons is clearly important, as is shown by the change from an ^{241}Am-Be to a ^{252}Cf spectrum. To see the effect of small changes in the starting spectrum, tallies were run with ISO spectra modified to reassign approximately 5% of the emission probability of the 2nd lowest energy bin to the lowest bin, and from the 4th to the 3rd, the 6th to the 5th and so on. Although this technique for estimating uncertainties is not ideal, it does allow for possible misallocation of fluence in the unfolding of the spectrum, and gives an indication of the sensitivity of the corrections to the energy spectrum of the source.

All uncertainties given in the following tables correspond to a 67% confidence level (1σ). The total uncertainties were found by adding the components in quadrature. Contributions to the overall source emission rate uncertainty were calculated from the values in table 2 in accordance with UKAS publication M3003[UK97].

Table 8: Uncertainties in oxygen and sulphur fast neutron capture [O]

	Uncertainty (%)		
	^{252}Cf X1	^{241}Am-Be X3	^{241}Am-Be X14
Statistical	0.3	0.2	0.2
Cross section	15	20	20
Geometry	0.2	0.3	0.3
Source energy spectrum	0.04	0.03	0.03
Total	15	20	20
Contribution to uncertainty in source emission rate	0.07	0.40	0.40

Table 9: Uncertainties in source and cavity capture [S]

	Uncertainty (%)		
	^{252}Cf X1	^{241}Am-Be X3	^{241}Am-Be X14
Statistical	0.5	0.5	0.5
Cross section	3	3	3
Geometry	3.1	3.0	3.0
Source energy spectrum	0.1	0.03	0.03
Total	4.3	4.3	4.3
Contribution to uncertainty in source emission rate	0.05	0.04	0.05

Table 10: Uncertainties in neutron leakage from the bath [L]

	Uncertainty (%)		
	^{252}Cf X1	^{241}Am-Be X3	^{241}Am-Be X14
Statistical	1.4	0.7	0.7
Cross section	6	3	3
Geometry	1.6	1.4	1.4
Source energy spectrum	0.03	0.2	0.2
Total	6.4	3.4	3.4
Contribution to uncertainty in source emission rate	0.01	0.03	0.03

The total uncertainty in O and L is dominated by the cross section component. The geometry uncertainty is equally significant in the case of capture by the source and cavity. Of the two geometry perturbations, the change in solution density had a far greater effect than the change in the steel specification, even in the value of S.

Only the O correction for ^{241}Am-Be sources contributes significantly to the uncertainty in the source emission rate. The high value assigned to the cross section uncertainty for oxygen and sulphur fast capture could be reduced in the future if new evaluations of the O(n,α) cross section are in agreement with the ENDF/B-VI tables.

The results show that the calculations are not very sensitive to small changes in the source energy spectrum.

8 CONCLUSION

The work detailed in this report provides the necessary scientific evidence for the confident implementation of MCNP calculated correction factors in the determination of source emission rates by the manganese bath method.

Significant disagreement has been found between the correction factors obtained using the in-house codes and those calculated using MCNP. This has implications for sources measured previously at NPL and should be addressed separately.

The areas of disagreement between the two calculation methods have been investigated and resolved satisfactorily. Use of the MCNP model is further supported by the results of the experimental validation work.

Although the leakage correction factor should be determined using MCNP, it is proposed that the long counter be retained as a monitor of neutrons escaping from the bath. This will alert of any contamination of the source material which changes the energy spectrum and consequently alters the fraction of neutrons which escape.

9 FURTHER WORK

The model can now be adapted to cover the full range of source and capsule types, and also to include the large source cavity for capsules too big to fit in the small cavity. Variance reduction techniques should be incorporated into the model to reduce the time taken for convergence.

The production of the MCNP input file could be done by a simple program where the user specifies source and capsule type, and solution concentration. The program would calculate the atomic fractions for the solution as well as the density and the appropriate number densities for the tally multipliers. Another program could read the important information from the MCNP output file, then process it to produce a clear breakdown of neutron capture and loss.

A more detailed sensitivity analysis, building on the work described in section 7 of this report, should be carried out for the cross section data. This requires information on the uncertainties in the evaluated values which is not readily available for all isotopes and reaction types.

10 REFERENCES

[He94] Hendricks J S, Frankle S C, Court J D, 1994, *ENDF/B-VI Data for MCNP* (LA-12891)

[Sm95] Smith D, Woods S A, 1995, *Recommended Nuclear Decay Data* (NPL Report RSA[EXT]53)

[Ax65] Axton E J, Cross P, Robertson J C, 1965, Calibration of the NPL Standard Ra-Be Photoneutron Source by an Improved Manganese Sulphate Bath Technique, *J. Nucl. Energy* **19** pp409-22

[We58] Westcott C H, Walker W H, Alexander T K, 1958, *in: Proceedings of the Second International Conference on the Peaceful Uses of Atomic Energy, Geneva* (United Nations, New York) **16** pp70-6

[Ax85a] Axton E J, Bardell A G, 1985, Neutron Yield from the Spontaneous Fission of ^{252}Cf, *Metrologia* **21** pp59-74

[Ax85b] Axton E J, Bardell A G, Felgate S J, Long S M R, 1985, The Ratio of the Thermal Neutron Capture Cross-Sections for Hydrogen and Manganese and its Impact on the Measurement of Neutron Source Emission Rates by Manganese Bath Techniques, *Metrologia* **21** pp181-91

[Br97] Briesmeister J F, Ed., 1997, *MCNP – A General Monte Carlo N-Particle Transport Code, Version 4B* (LA-12625-M)

[Na94] Naismith O F, 1994, MCNP Calculation of Corrections for Manganese Bath Measurements (internal document)

[We73] Weast R C, Ed., 1973, *Handbook of Chemistry and Physics 53rd Edition* (CRC Press) F-131

[IS89] International Standard ISO 8529, 1989, Neutron Reference Radiations for Calibrating Neutron-Measuring Devices used for Radiation Protection Purposes and for Determining their Response as a Function of Neutron Energy, *International Organization for Standardization*, Geneva, Switzerland

[Sa73] Saclay Data Centre, 1973, private communication

[Ax86] Axton E J, 1986, The Thermal-Neutron Capture Cross-Sections of Mn and S, *J. Nucl. Energy* **11** pp627-628

[Ha91] Hale G M, Young P G, Chadwick M B, Chen Z –P, 1991, New Evaluations of Neutron Cross Sections for ^{14}N and ^{16}O, *Proc. Int. Conf. on Nuclear Data for Science & Technology, Germany* (Springer) pp921-3

[Br00] Briesmeister J F, Ed., 2000, *MCNP – A General Monte Carlo N-Particle Transport Code, Version 4C* (LA-13709-M)

[Ax63] Axton E J, 1963, Absolute Measurement of the Neutron Flux Density in the A.E.R.E. Reactor GLEEP, *Reactor Science and Technology (Journal of Nuclear Energy Parts A/B)* **17** pp125-35

[UK97] The Expression of Uncertainty and Confidence in Measurement, M3003, 1st Edition, 1997 (United Kingdom Accreditation Service)

The following is the MCNP input file for a 1 Ci ^{241}Am-Be source in an X3 capsule. The hydrogen to manganese atomic ratio (N_H/N_{Mn}) of the manganese sulphate solution is 33.200.

```
LARGE Mn BATH WITH Am-Be X3 SOURCE 17.7.00 (revised cavity&rod dimensions)
1     1  -7.93  1 -2 #(-16 14) #(-36 -25)       $ cavity shell
2     1  -7.93  (3 -4) #(-6 14)                 $ bath shell
3     0  5                                      $ neutron termination
4     1  -7.93  (16 -17 -10 2 14):(11 -17 10 -5) $ cavity transport rod
7     0  (-1:(-16 -10 1 14):(-11 10 -5)) #11 #12 #(-36 -25 -1) #18
                                                $ inside cavity
8     2  -1.4046  (2 -3) #(-17 14) #(-24 2 19 -18) #(2 -36 31 -33) #16 #17
                                                $ MnSO4
9     3  -2.02  22 -23 21 -20                   $ cavity seal O-ring
10    1  -7.93  (2 -24 19 -18) #9               $ cavity seal
11    4  -1.24  -29 27 -26                      $ source material
12    1  -7.93  (-28 25 -37) #11                $ source capsule
13    0  -32 -25 33                            $ source rod (inside)
14    1  -7.93  (-36 -25 31) #13                $ source rod
15    0  (-5 4) #(-17 14)                       $ outside bath
16    1  -7.93  2 18 -34 -35 17 #17             $ cavity vacuum cup
17    3  -2.02  2 -9 7 -8 14                    $ cavity vacuum cup O-ring
18    1  -7.93  (28 -38 -41 40):(36 -28 -25 40) $ source cup
20    1  -15.9  (3 -4 -6 14) #(-17 14)          $ bath lid

1     SO  4.344           $ internal surface of cavity sphere
2     SO  4.4             $ external surface of cavity sphere
3     SO  50              $ internal surface of bath shell
4     SO  50.15           $ external surface of bath shell
5     SO  70              $ boundary sphere surface
6     CZ  15.22           $ edge of bath lid
7     CZ  1.13            $ internal radius of vacuum cup O-ring
8     CZ  1.42            $ external radius of vacuum cup O-ring
9     SO  4.58            $ upper surface of vacuum cup O-ring
10    PZ  7.8             $ upper surface of vacuum cup joint
11    CZ  0.47            $ internal surface of transport rod above joint
14    PZ  4               $ ambiguity surface
16    CZ  0.33            $ internal surface of cavity transport rod
17    CZ  0.65            $ external surface of cavity transport rod
18    PZ  0.35            $ upper surface of cavity seal
19    PZ  -0.45           $ lower surface of cavity seal
20    PZ  0               $ upper surface of cavity O-ring
21    PZ  -0.22           $ lower surface of cavity O-ring
22    CZ  4.65            $ inside edge of cavity O-ring
23    CZ  4.95            $ outside edge of cavity O-ring
24    CZ  5.28            $ outside edge of cavity seal
25    PZ  -1.46           $ bottom of source capsule
26    PZ  0.815           $ top of source material
27    PZ  -0.815          $ bottom of source material
28    CZ  1.12            $ outside edge of source capsule
29    CZ  0.88            $ inside edge of source capsule
31    PZ  -4.6            $ bottom of source rod
32    CZ  0.2             $ inner surface of source rod
33    PZ  -3.334          $ inner bottom surface of source rod
34    CZ  1.65            $ side edge of cavity vacuum cup
35    SO  4.75            $ upper surface of cavity vacuum cup
36    CZ  0.303           $ outer edge of source rod
37    PZ  1.39            $ top of source capsule
38    CZ  1.19            $ outer edge of source cup
40    PZ  -1.51           $ outer surface of source cup base
41    PZ  -0.49           $ inner surface of source cup base
42    SO  1.84011         $ source emission sphere

IMP:N 1 1 0 1 13R
C
SC1   Am-Be SPECTRUM (ISO 8529)
SDEF  ERG=D1 SUR=42
SI1   H  4.14E-07 0.11 0.33 0.54 0.75 0.97 1.18 1.4 1.61 1.82 2.04
      2.25 2.47 2.68 2.9 3.11 3.32 3.54 3.75 3.97 4.18 4.39 4.61
      4.82 5.04 5.25 5.47 5.68 5.89 6.11 6.32 6.54 6.75 6.96 7.18
      7.39 7.61 7.82 8.03 8.25 8.46 8.68 8.89 9.11 9.32 9.53 9.75
      9.96 10.18 10.39 10.6 10.82 11.03
```

```
SP1   D 0  0.0144 0.0334 0.0313 0.0281 0.025 0.0214 0.0198 0.0175
      0.0192 0.0222 0.0215 0.0225 0.0228 0.0295 0.0356 0.0368
      0.0346 0.0307 0.03 0.0269 0.0286 0.0318 0.0307 0.0333 0.0304
      0.0274 0.0233 0.0206 0.0181 0.0177 0.0204 0.0183 0.0163
      0.0168 0.0168 0.0188 0.0184 0.0169 0.0143 0.0097 0.0065
      0.0043 0.0037 0.0038 0.0051 0.0062 0.0055 0.0047 0.0037
      0.0028 0.0015 0.0004
C
FC1   NEUTRON LEAKAGE FROM BATH
F1:N  5
FC11  THERMAL ENERGY SPECTRUM INSIDE CAVITY
F11:N 1
E11   1.0E-09 1.0E-07 5.0E-07 20
FC21  THERMAL ENERGY SPECTRUM OUTSIDE CAVITY
F21:N 2
E21   1.0E-09 1.0E-07 5.0E-07 20
FC4   NEUTRON CAPTURE IN CAVITY
F4:N  1 4 10 12 14 16 18 T
FM4   8.62157E-02 1 -2
FC14  NEUTRON CAPTURE IN RUBBER SEAL
F14:N 9
FM14  0.225073 3 -2
FC24  NEUTRON CAPTURE IN MnSO4 SOLUTION
F24:N 8
FM24  1.04936E-01 2 -2
FC34  (N,GAMMA) CAPTURE IN MANGANESE
F34:N 8
FM34  1.878E-03 5 -2
FC44  NEUTRON CAPTURE IN SULPHUR: TOTAL, (N,GAMMA), (N,P), (N,ALPHA)
F44:N 8
FM44  1.878E-03 6 (-2) (102) (103) (107)
FC54  NEUTRON CAPTURE IN OXYGEN:  TOTAL, (N,GAMMA), (N,ALPHA)
F54:N 8
FM54  3.874E-02 7 (-2) (102) (107)
FC64  (N,GAMMA) CAPTURE IN HYDROGEN
F64:N 8
FM64  6.243E-02 8 -2
FC74  NEUTRON CAPTURE IN SOURCE MATERIAL
F74:N 11
FM74  7.816E-02 4 -2
C
M1    26000 -0.65395 24000 -0.17 28000 -0.12 25055 -0.02 14000 -0.01
      15031 -0.00045 16032 -0.0003 6012 -0.0003 42000 -0.025  $ STEEL
M2    25055 0.0179 16032 0.0179 8016 0.0717
      1001 0.5950 8016 0.2975              $ MnSO4 SOLUTION
M3    6012 0.4 1001 0.6                    $ RUBBER
M4    95241 0.00220 4009 0.99339 8016 0.00441  $ SOURCE MATERIAL
M5    25055 1                                $ MANGANESE
M6    16032 1                                $ SULPHUR
M7    8016 1                                 $ OXYGEN
M8    1001 1                               $ HYDROGEN
MT2   LWTR.01
C
PHYS:N  20 20
C
NPS  1500000
```